UHASSELT
KNOWLEDGE IN ACTION

Maastricht University

Faculty of Medicine and Life Sciences
School for Life Sciences
Master of Biomedical Sciences

Master's thesis

Lysosomal stress and cathepsin dysregulation in Charcot-Marie-Tooth Disease Type 1A

Jochim Martens

Thesis presented in fulfillment of the requirements for the degree of Master of Biomedical Sciences, specialization Molecular Mechanisms in Health and Disease

SUPERVISOR :

Prof. dr. Esther WOLFS

MENTOR :

Mevrouw Hanne JEURISSEN

2024
2025

Transnational University Limburg is a unique collaboration of two universities in two countries: the University of Hasselt and Maastricht University.

UHASSELT
KNOWLEDGE IN ACTION

www.uhasselt.be
Universiteit Hasselt
Campus Hasselt:
Martelarenlaan 42 | 3500 Hasselt
Campus Diepenbeek:
Agoralaan Gebouw D | 3590 Diepenbeek

Faculty of Medicine and Life Sciences
School for Life Sciences
Master of Biomedical Sciences

Master's thesis

Lysosomal stress and cathepsin dysregulation in Charcot-Marie-Tooth Disease Type 1A

Jochim Martens

Thesis presented in fulfillment of the requirements for the degree of Master of Biomedical Sciences, specialization Molecular Mechanisms in Health and Disease

SUPERVISOR :

Prof. dr. Esther WOLFS

MENTOR :

Mevrouw Hanne JEURISSEN

Lysosomal Stress and Cathepsin Dysregulation in Charcot-Marie-Tooth Disease Type 1A

Martens J.[1], Jeurissen H.[2], Libberecht K.[2,3,4], and Wolfs E.[2]

[1]UHasselt, Faculty of Medicine and Life Science, Agoralaan, 3590 Diepenbeek, Belgium.
[2]UHasselt, Lab for Functional Imaging & Research in Stem cells (FIERCE lab), BIOMED, Agoralaan, 3590 Diepenbeek, Belgium.
[3]VIB, Center for Brain & Disease Research, Laboratory of Neurobiology, Leuven, Belgium
[4]KU Leuven, Department of Neurosciences, Experimental Neurology, and Leuven Brain Institute

*Running title: *"Navigating the Silent Disruptor: Cathepsins in CMT1A"*

Address for correspondence: Prof. Dr. Esther Wolfs, Tel: +32 11 26 92 96; Email: esther.wolfs@uhasselt.be

Keywords: Charcot-Marie-Tooth disease type 1A, Schwann cells, PMP22, Lysosomes, Cathepsin B/D

ABSTRACT

Charcot-Marie-Tooth disease type 1A (CMT1A), the most common inherited peripheral neuropathy, is caused by PMP22 gene duplication, leading to myelin instability, Schwann cell dysfunction, and axonal degeneration. While the genetic basis - PMP22 duplication - is well understood, the downstream cellular mechanisms remain unclear. This study investigates whether lysosomal dysfunction and cathepsin upregulation - particularly of cathepsin B and D (CtB & CtD) - drive extracellular matrix (ECM) degradation and contribute to Schwann cell pathology in CMT1A. To evaluate protease function of cathepsins and myelin pathology, we used both human iPSC-derived Schwann cell precursors (iPSC-SCP) and the C3-PMP22 transgenic mouse model. Findings revealed elevated expression of CtB and CtD in CMT1A models, with significantly increased ECM degradation in conditioned medium from iPSC-SCP. Recombinant protease assays confirmed cathepsin-mediated collagen IV breakdown. However, pharmacological inhibition only partially reduced ECM degradation, suggesting the involvement of additional enzymatic activities or parallel degradation pathways. These results implicate lysosomal leakage and cathepsin dysregulation as pathological mechanisms in CMT1A. Using DQ-collagen assays, we observed increased ECM degradation in CMT1A conditions. qPCR revealed upregulation of lysosomal and inflammatory genes, while immunofluorescence confirmed elevated expression and altered localization of CTB, CTD, and LAMP1. Transmission electron microscopy further showed disrupted myelin architecture and signs of axonal degeneration in CMT1A nerve tissue. While single-pathway inhibition was insufficient, compounds like C381 that restore lysosomal homeostasis may offer broader therapeutic benefits. Targeting both upstream stress and downstream protease activity could support the development of an effective, disease modifying treatment for CMT1A and other demyelinating diseases.

INTRODUCTION

***Background on CMT and its clinical relevance* -** Charcot-Marie-Tooth disease (CMT), also referred to as hereditary motor and sensory neuropathy (HMSN), is the most prevalent inherited peripheral neuropathy, affecting approximately 1 in 2,500 individuals globally (1, 2). This disorder primarily impairs both sensory and motor nerves, resulting in clinical manifestations such as muscle weakness, muscle atrophy in the distal extremities, distal sensory loss, diminished or absent deep tendon reflexes, and foot deformities, including pes cavus, foot drop, and hammertoes (3). Symptoms of CMT typically appear within the first two decades of life and progressively worsen, advancing in a proximal and ascending manner (3). Collectively, CMT encompasses a heterogeneous group of disorders that primarily target the peripheral nervous system (PNS), underscoring its genetic and phenotypic complexity (4). Currently, there is no cure available for CMT. Instead, disease management relies on supportive measures,

including rehabilitative therapy, orthopedic devices, and surgical interventions to address skeletal deformities and soft-tissue abnormalities, which help alleviate symptoms. This highlights the urgent need to advance our understanding of CMT pathogenesis, especially in subtypes as CMT1A, to facilitate the development of targeted, disease-modifying treatments (1, 3).
Classification of CMT is based on inheritance patterns and the nature of nerve damage, as identified through nerve conduction studies (NCS). CMT1, the demyelinating form, is characterized by slowed nerve conduction velocities (NCVs) of less than 38 m/s, while CMT2, the axonal form, exhibits primary axonal degeneration with mildly reduced NCVs ranging from 38 to 45 m/s (3, 5). Advances in next-generation sequencing (NGS) have significantly expanded our understanding of the genetics underlying CMT, identifying over 100 causative genes and mutations. Despite this progress, genetic heterogeneity results in overlapping clinical phenotypes, complicating classification and bedside diagnosis. Notably, around 90% of genetically diagnosed CMT cases are linked to mutations in one of four predominant genes: *PMP22* (*peripheral myelin protein 22*) duplication in CMT1A, *MPZ* (*myelin protein zero*) in CMT1B, *GJB1* (*gap junction protein beta 1*) in CMT1X, and *MFN2* (*mitofusin 2*) in CMT2A (2).

PMP22 gene duplication - Charcot-Marie-Tooth disease type 1A (CMT1A) is the most prevalent subtype of CMT, accounting for nearly 80% of all demyelinating cases. It is caused by a 1.4 tandem duplication on chromosome 17p11.2, encompassing the *PMP22* (*peripheral myelin protein 22*) gene (1, 6, 7). *PMP22*, a 22-kDa tetraspan hydrophobic aggregation-prone glycoprotein, accounts for approximately 2-5% of the total myelin proteins in the peripheral nervous system (PNS) and is primarily expressed by Schwann cells, the glial cells responsible for myelination in the PNS (6, 8). Although its exact function remains unknown, PMP22 is known to play critical roles in Schwann cell differentiation, growth, myelin stabilization, and the establishment of lipid rafts, which are essential for maintaining the integrity and functionality of myelin (9-12).

PMP22 comprises six exons and generates two transcripts (exon-1a and exon-1b) via distinct promoters, producing unique 5' untranslated regions (6). Its expression is widespread during embryogenesis but later peaks in myelinating Schwann cells, with minimal "Central Nervous System White Matter" (CNS) expression. Exon-1a predominates in the sciatic nerve, while exon-1b is more abundant in the brainstem, spinal cord, muscle, and heart (6). Precise regulation of PMP22 is essential for myelin stability; its dysregulation - through overexpression, deletion, or mutation - disrupts Schwann cell function and underlies CMT1A pathology (6, 8).

Molecular pathophysiology of Schwann cells - In CMT1A, PMP22 overexpression leads to an increase in intracellular PMP22 compared to the amount trafficked to the cell surface, resulting in misfolding and the formation of protein aggregates within Schwann cells (13, 14). This disrupts normal cellular processes, leading to widespread dysmyelination, myelin sheath defects, shorter internodes, and axonal loss (8, 15). Under normal physiological conditions, only 20% of newly synthesized PMP22 is successfully folded and integrated into the myelin membrane, with the remaining 80% undergoing degradation to maintain proteostasis (9, 16, 17). The ubiquitin-proteasome system (UPS) serves as the primary pathway for degrading misfolded PMP22 by tagging it with polyubiquitin chains for proteasomal destruction (10, 11). However, in CMT1A, the overexpression of PMP22 overwhelms the UPS, leading to the accumulation of misfolded proteins in the endoplasmic reticulum (ER) (9, 18-20).
In response Schwann cells activate the unfolded protein response (UPR), which channels misfolded proteins to the cytosol for degradation by the ubiquitin-proteasome system (UPS). However, when the burden of misfolded or aggregated PMP22 exceeds UPS capacity, proteasomal degradation becomes insufficient, leading to protein accumulation and cellular stress (10, 21-28). To cope with this overload, Schwann cells engage the autophagy-lysosomal pathway (ALP) as a compensatory degradation mechanism. Nevertheless, this response is often inadequate, resulting in lysosomal stress, impaired trafficking, and reduced protein clearance - all of which contribute to Schwann cell

dysfunction and disease progression in CMT1A (9-12). PMP22 overexpression also disrupts lipid metabolism, suppressing cholesterol biosynthesis, decreasing sphingomyelin levels, and elevating ceramide concentrations. These alterations destabilize lipid rafts, which are critical cholesterol-enriched plasma membrane microdomains involved in Schwann cell signaling (8). Cholesterol is essential for maintaining the stability of the lipid-rich myelin membrane, and its dysregulation, along with excessive lipid droplet accumulation in lysosomes, impairs lipid recycling. This further weakens Schwann cell support for axons, promoting demyelination and axonal degeneration (8). The interplay between proteostasis collapse and lipid dysregulation creates systemic cellular stress within Schwann cells, driving the hallmark features of CMT1A: progressive demyelination and axonal degeneration.

Lysosomal dysfunction and the role of Cathepsins in CMT1A - Lysosomes are acidic, membrane-bound organelles that act as the primary degradative compartments of the cell. They maintain intracellular homeostasis by breaking down cellular waste, including proteins, lipids, and damaged organelles. This is achieved through a diverse set of hydrolytic enzymes located within the lysosomal lumen, such as proteases, nucleases, and lipases (29). A primary route through which cellular waste reaches the lysosome is macroautophagy. During this process, cytoplasmic material such as misfolded proteins, protein aggregates, and damaged organelles are stored in double-membrane vesicles called autophagosomes. These fuse with lysosomes, causing the content to be enzymatically degraded. Macroautophagy thus plays an important role in regulating protease and cellular homeostasis (29,30). Among the key lysosomal enzymes are cathepsins, a large family of proteases that mediate protein degradation both inside and outside the lysosome (30). These enzymes are synthesized as inactive pro-cathepsins in the endoplasmic reticulum (ER), glycosylated in the Golgi, and trafficked to lysosomes where they are activated in the acidic lumen maintained by vacuolar H+-ATPase (31). Cathepsins are subdivided into three classes based on their catalytic mechanism: Cysteine proteases (e.g., cathepsin B, L, S), Aspartic proteases (e.g., cathepsin D, E), and Serine proteases (e.g., Cathepsin G). While their primary role in intracellular protein degradation, cathepsins also contribute to extracellular matrix (ECM) remodeling, cell-cell adhesion disruption, and even inflammation when released extracellularly (30). In the context of CMT1A pathology, particular attention has been given to the role of cathepsin B (CtB) and D (CtD). These enzymes are capable of degrading ECM components and disease progression. CtB degrades structural ECM components like collagen and fibronectin and is implicated in pathological conditions such as tumor invasion, metastasis, and neurological diseases like Alzheimer's, where it contributes to amyloid plaque formation (30). CtD targets proteins like fibronectin and laminin and is involved in immune regulation, protein recycling via the MHC class II pathway, and apoptosis, with ceramide acting as an activator (32-37). In CMT1A, lysosomal and autophagic markers colocalize with PMP22 aggregates, indicating activation of the ALP (12). Yet, this response is insufficient to fully degrade accumulated proteins, resulting in lysosomal stress. Over time, this stress can compromise lysosomal membrane integrity, leading to lysosomal membrane permeabilization (LMP) and the release of cathepsins into the cytosol and extracellular space (31, 38). This process is regulated by lysosomal-associated membrane proteins (LAMPs), particularly LAMP1, which modulate lysosomal fusion and exocytosis (14, 15, 38). The extracellular activity of cathepsins such as CtB and CtD may contribute significantly to ECM breakdown and Schwann cell destabilization in CMT1A (***Fig. 1***).

Lysosomal Integrity and Cathepsin Activity - Lysosomal stress and cathepsin dysregulation have been linked to Schwann cell pathology in CMT1A. This is evidenced by increased lysosomal size, activity, and permeability, observed in both *in vitro* and *in vivo* models. For example, Schwann cells differentiated from human dental pulp stem cells (DPSCs) exhibited heightened lysosomal vulnerability under stress conditions induced by chloroquine, showing increased lysosomal size and permeability along with reduced cell viability. Similarly, primary mouse Schwann cells derived from CMT1A models

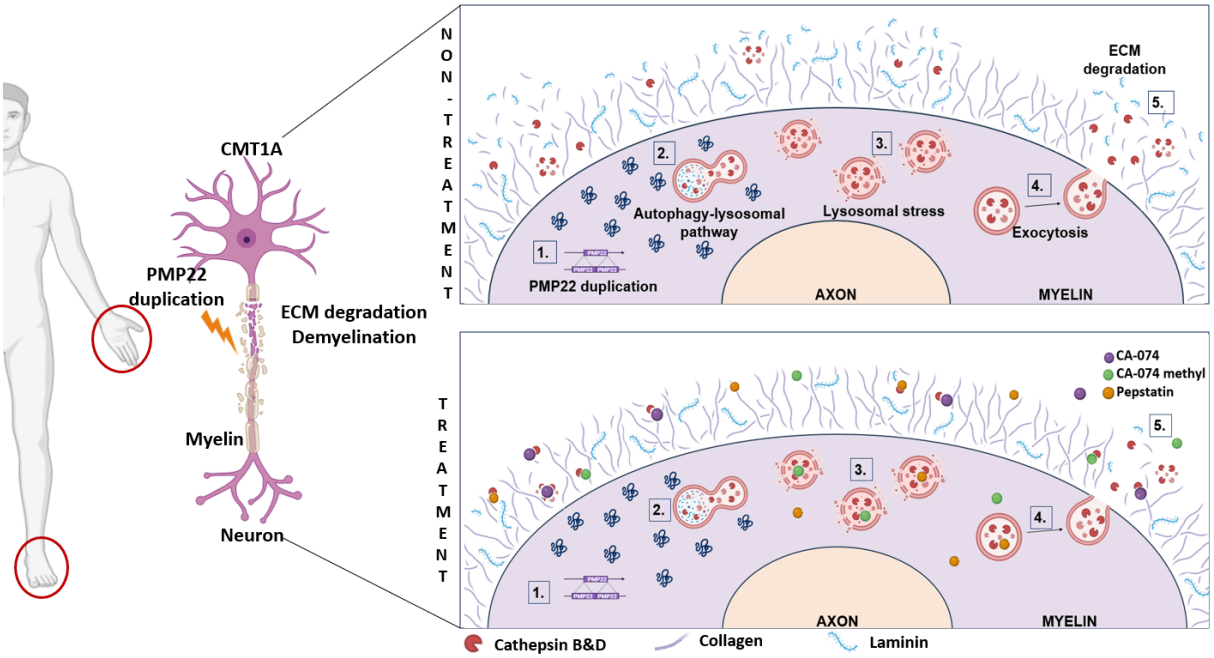

Fig. 1: Schematic representation of Charcot-Marie-Tooth disease type 1A (CMT1A) and its pathological mechanisms with and without treatment. CMT1A is caused by PMP22 gene duplication, leading to extracellular matrix (ECM) degradation, demyelination, and nerve deterioration. The top panel (CMT1A) illustrates the disease progression, including increased autophagy-lysosomal pathway activation, lysosomal stress, excessive exocytosis, and ECM degradation. The bottom panel (including treatment) demonstrates the effects of therapeutic agents (CA-074, CA-074 methyl, and Pepstatin), which are hypothesized to mitigate lysosomal stress, reduce exocytosis, and prevent ECM degradation, thereby preserving nerve function.

demonstrated comparable lysosomal dysfunction. *In vivo* studies using the C3-PMP22 mouse model further revealed progressive lysosomal permeability in sciatic nerves, coupled with elevated expression of lysosomal stress markers (*Libberecht, K. Unpublished PhD thesis, 2024*). This lysosomal dysfunction correlates with dysregulated activity of cathepsins, particularly CtB and CtD. Increased intracellular and extracellular activity of these enzymes was observed, driven by lysosomal membrane permeabilization that released them into the extracellular environment. Once extracellularly present, these enzymes contribute to ECM remodeling by degrading structural components such as collagen, fibronectin, and laminin. This remodeling disrupts Schwann cell-axon interactions, destabilizing nerve architecture and accelerating nerve degeneration. Together, these findings underscore the role of lysosomal dysfunction and cathepsin activity in Schwann cell degeneration and peripheral nerve damage in CMT1A.

To modulate cathepsin activity, selective inhibitors with different properties are used. CA-074 is a specific, cell-impermeable inhibitor that primarily targets CtB extracellularly. Its derivative, CA-074 methyl ester (CA-074Me), is membrane-permeable and inhibits CtB intracellularly. In contrast, Pepstatin A, a broad spectrum aspartic protease inhibitor targets CtD (***Fig. 1***).

Additionally, C381, a benzyl urea derivative, will be tested for its potential to improve lysosomal homeostasis. C381 has demonstrated neuroprotective and anti-inflammatory properties in multiple models of neurodegeneration and vascular injury. It is orally bioavailable, blood–brain barrier permeable (ClogP = 3.3), and activates TGF-β signaling while enhancing lysosomal acidification and function by interacting with the vacuolar H^+-ATPase proton pump on the lysosomal membrane (39, 40). These properties allow C381 to improve the clearance of aggregated proteins and reduce inflammation. Although C381 has not yet been tested in CMT1A, its mechanistic alignment with key disease processes—notably lysosomal dysfunction, ER stress, and inflammatory cascades—suggests therapeutic potential. In particular, C381 may indirectly impact the PERK (PKR-like ER kinase) pathway, which is activated by ER stress in Schwann cells as a response to excessive misfolded PMP22. Chronic activation of

PERK impairs protein synthesis and promotes apoptosis, contributing to Schwann cell dysfunction and myelin instability (41). By enhancing lysosomal clearance and reducing the burden on the ER, C381 may attenuate PERK pathway activation, thereby promoting Schwann cell survival and preserving nerve integrity.

Disease Models and Research Advances - Developing accurate CMT1A models is challenging due to its genetic complexity and human-specific pathology. Early models, like the Trembler J mouse with a PMP22 point mutation, provided insights into demyelination but failed to replicate human CMT1A, which results from PMP22 duplication (42). To address this, transgenic models such as the C22 mouse (seven PMP22 copies via YAC) were created, closely mimicking gene duplication but exhibiting a more severe phenotype (43). The C3 mouse (three to four copies) presents a milder, more clinically relevant phenotype (44). However, rodent models struggle to predict human treatment outcomes, as seen with ascorbic acid's clinical trial failure despite promising rodent results (45). To overcome these limitations, patient-derived iPSCs differentiated into Schwann cell precursors (iPSC-SCPs) offer an *in vitro* system that replicates CMT1A pathology. iPSC-SCPs are used as a valuable alternative because isolating primary Schwann cells (SCs) from human peripheral nerves is not ethically or practically feasible. This patient-in-a-dish model gives the opportunity to examine immature SCs with patient-specific genotypes which allows to investigate disease progression and cellular responses relevant to humans.(42). Combined with models like C3-PMP22 mice, iPSC systems enhance validation efforts.

This study hypothesizes that lysosomal dysfunction and cathepsin-mediated ECM remodeling drive Schwann cell dysfunction and nerve degeneration in CMT1A. It investigates how CtB and CtD release impacts lysosomal integrity, ECM degradation, and downstream effects on Schwann cell and axonal stability, and whether their inhibition can mitigate these effects. Using human *in vitro* models and the C3 mouse model, the therapeutic potential of CtB and CtD inhibition will be assessed. Additionally, the study will evaluate C381, a small molecule that enhances TGF-β signaling and lysosomal function, as a potential disease-modifying treatment. By targeting protein aggregation, ER and lysosomal stress, and inflammation, C381 addresses multiple CMT1A pathomechanisms. Its effects will be tested in iPSC-derived Schwann cell precursors and the C3 mouse model to determine its therapeutic efficacy.

EXPERIMENTAL PROCEDURES

Culturing iPSC-SCP and conditioned medium (CM) collection – iPSC-SCPs were cultured on Matrigel®Matrix(MG)-coated (Corning, 356231) flasks in a 1:1 mixture of DMEM/F12 (Thermofisher, 10565018) and Neurobasal (Thermofisher, 21103049) medium supplemented with 2 mM Glutamax (Thermofisher, 35050061), 1% N2 (Thermofischer, 17502048), 2% B27 (Thermofisher, 12587010), 20 µM SB431542 (Tocris, 1614), 3 µM CHIR99021 (Tocris, 4423), 13.3 µM Neuregulin-1 (Peprotech, 100-03), 0.005% bovine serum albumin (Enzo Life Sciences BVBA, 11930), 0.11 mM β-mercaptoethanol (Gibco, 31350-010), and 1% penicillin-streptomycin (Thermofisher, 15140122). In this study, we primarily used pre-differentiated iPSC-SCPs generously provided by Prof. Dr. Ludo Van Den Bosch (VIB-KU Leuven, Belgium). SCPs were thawed from cryopreserved stocks stored in 90% knockout serum and 10% DMSO (PanRcac AppliChem, A3672-0100), resuspended in SCP medium, and seeded at a density of 500,000 cells per flask, cultured in standard conditions (37°C, 5% CO_2). After 72 hours, conditioned medium (CM) was collected and centrifuged at 15000 rpm for 10 min at 4°C. Samples were stored at -80°C until further notice. After CM collection, cells were washed with PBS (Capricorn scientific, CP25-817), enzymatically detached, and counted. Cell pellets were then lysed in a RIPA buffer containing protease inhibitors (Roche Diagnostics, Indianapolis, IN) for 20 minutes on ice. Lysates were centrifuged at 13.000 rpm for 10 minutes at 4°C, and the resulting supernatants were stored at -80°C for subsequent protein analysis.

DQ collagen degradation assay – Three different ECM-mimicking coatings were used: Laminin (Merck, L2020), Laminin with DQ collagen type IV (Invitrogen, D12052), and

Laminin with DQ collagen (with an additional amount of DQ collagen added after a three-hour incubation period), all in DMEM/F12. After three hour incubation, an additional amount of DQ collagen was added to each well (except MG-coated wells). Furthermore, collagenase treatment serves as a positive control. ISO and CMT cells were seeded at a density of 15,000 cells per well and maintained at 37°C for 24 hours. Collagen degradation was assessed by treating selected wells with collagenase at a 1:500 dilution, with incubation periods of either 24 hours and one hour. Following treatment, fluorescence intensity was measured using a CLARIOstar® Plus plate reader to assess DQ collagen cleavage, indicating enzymatic degradation activity. This approach allowed a comprehensive assessment of ECM degradation dynamics by CM and collagenase treatment.

In vivo study – Heterozygote C3-PMP22 mice and wild-type C57BL/6J mice, kindly provided by Prof. Dr. Frank Baas (LUCM, the Netherlands), were bred and housed according to the guidelines of Hasselt University, with five to ten animals per cage in a temperature-controlled environment (±20°C) under a 12-hour light/dark cycle and *ad libitum* access to food and water. All experimental procedures were conducted in accordance with institutional and national ethical guidelines and were approved by the Ethical Committee for Animal Experimentation (ECAE) of Hasselt University. Genotyping was performed on ear biopsies using PCR to identify human PMP22. The following primer pair was used: forward (F) 5'-TGG TGA TGA TGA GAA ACA GT-3' and reverse (R) 5' -TGA TTC TCT CTA GCA ATG GA- 3'.

All compounds used, including C381 (new *in vivo)* (Selleckchem, S6654), were dissolved in 10% dimethyl sulfoxide (DMSO) and further diluted using appropriate co-solvents, such as 40% PEG300 (Selleckchem, S670421), 5% Tween-80 (Selleckchem, S670217), and 45% ddH_2O, to achieve the required working concentrations. Solutions were freshly prepared before administration. CA-074 (EC) (MCE, HY-103350) and CA-074 methyl ester (IC) (MCE, HY-100350) were prepared at 2.5 mg/ml and 2 mg/ml, respectively, while Pepstatin (MCE, HY-P0018) was also prepared at 2 mg/ml. The working concentration of C381 is 3mg/mL. Two vehicle solutions were formulated to match the dosing regimens, and mice received intraperitoneal (IP) injections of the assigned compound or vehicle according to group allocation.

To assess motor function and neuromuscular coordination, a series of behavioral tests were conducted. In the Rotarod test, mice were placed on an accelerating rotating rod (4 to 50 rpm), and the latency to fall (or spin three times around the rod) was recorded as a measure of motor coordination and balance. The beam walk test required mice to transverse a narrow beam (12 mm and 7 mm) three times as fast as possible to record speed and balance. Forelimb grip strength and endurance were assessed using the hanging wire test, where mice were suspended from a grid, and the time until they released was measured. Additionally, the clasping phenotype was evaluated by lifting the mice by the tail and observing limb positioning, as abnormal clasping behavior is indicative of neuromuscular impairment. All behavioral assessments were conducted by blinded researchers to ensure unbiased evaluation.

To further investigate neuronal function, electrophysiological recordings were performed to assess synaptic function and neuronal excitability. Mice were anesthetized using isoflurane, and recordings were conducted from the sciatic nerve. The recorded latency and amplitude were analyzed to identify functional alterations between WT and C3 mice.

Quantitative PCR (qPCR) – C3 and WT mice were sacrificed by cervical dislocation. Sciatic and brachial plexus nerves were snap frozen in liquid nitrogen and stored at -80°C before being pooled for further analysis. For RNA extraction, pooled nerve samples were homogenized using the NZY Total RNA Isolation Kit (NZYTech) in combination with the QIAzol Lysis Reagent (Qiagen, Hilden, Germany). RNA concentration and purity were measured using a Nanodrop spectrophotometer (Thermo Fisher Scientific). Subsequently, 3 ng/µL cDNA was synthesized from RNA using Qscript (Quantabio, Beverly, MA, USA). For qPCR, SYBR Green master mix (Thermo Fisher Scientific, Applied Biosystems) was prepared with gene-specific primers

(***Supplementary Table 1***), and reactions were performed in triplicate. Primer efficiency was validated for all targets. The QuantStudio system (Thermo Fisher Scientific, Applied Biosystems) was used to record cycle threshold (Ct) values, and relative gene expression (fold change) was calculated after normalization by validated housekeeping genes.

Immunohistochemistry (IHC) – Sciatic nerves were snap-frozen in Tissue-Tek (Sakura) and stored at -80°C until sectioning. Coronal sections (20 µm thick) were prepared using Leica CM3050 S cryostat (Leica Biosystems, Wetzler, Germany) and stored at -80°C until further processing. For staining, sections were washed in PBS and blocked for one hour with 100% Dako Protein Block (serum-free) (Dako, X0909). Primary antibodies (***Supplementary Table 2***) were applied overnight at 4°C, while negative control sections were incubated with 10% Protein Block instead. Following primary antibody incubation, sections were treated for one hour in the dark with fluorescent secondary antibodies; Alexa Fluor 488 goat anti-rat (1:400, A11006), Alexa Fluor 555 goat anti-rabbit (1:400, A21428), Alexa Fluor 555 donkey anti-rabbit (1:400, A31572), and Alexa Fluor 647 goat anti-rat (1:400, A21247). After thorough PBS washes, nuclei were labeled with DAPI for 10 minutes at room temperature in the dark. Slides were then rinsed, excess PBS was carefully removed, and sections were mounted with Fluoromount for imaging. Fluorescence images were obtained using Leica DM400 B LED microscope and analyzed with ImageJ. Thresholding was applied to quantify the percentage of stained area (%Area) relative to the total nerve area, as well as the integrated density (%Area x mean fluorescence intensity). For each mouse, measurements were averaged across three to four representative nerve sections.

Statistical analysis - All statistical analyses were performed using GraphPad Prism version 10.4.2 (622). Prior to further analysis, the dataset was checked for outliers. This involved using the Grubbs' test (for most datasets) or the ROUT test (for TEM results), depending on the type of data. Next, the normality was evaluated using the Shapiro-Wilk test. If the data were normally distributed, parametric tests were applied: an unpaired t-test for comparison between two groups or a one-way ANOVA for more than two groups. When ANOVA showed significance, Tukey's multiple comparisons test was applied. If the data were not normally distributed, non-parametric equivalents were used: the Mann-Whitney U test (two groups) or the Kruskal-Wallis test for (multiple groups), followed by Dunn's test with Bonferroni correction for multiple comparisons. All data are presented as the mean ± standard error of the mean (SEM). Statistical significance was determined using the following p-value grades: * ($p \leq 0.05$), ** (($p \leq 0.01$), ***($p \leq 0.001$), and ****($p \leq 0.0001$).

RESULTS

Enhanced ECM degradation in CMT1A Schwann cells - CMT1A Schwann cell precursors display significantly elevated ECM-degrading activity driven by secreted cathepsins. To investigate whether factors secreted by iPSC-derived Schwann cell precursors (iPSC-SCPs) from CMT1A patients contribute to extracellular matrix (ECM) degradation, we performed a DQ-collagen assay using conditioned medium (CM) obtained from both CMT1A and isogenic control (ISO) cell lines. To simulate the ECM environment, a coating mixture of laminin and DQ-collagen type IV was performed, a quenched fluorogenic substrate that becomes fluorescent upon proteolytic cleavage. We hypothesized that proteases secreted into the CM, possibly cathepsins, would cleave DQ-collagen type IV, resulting in measurable fluorescence. In an initial setup, fluorescence was measured in the coated plate (where DQ-collagen type IV and CM were incubated together) and in a second plate where the medium was transferred after incubation. In the coated plate, no significant difference in fluorescence between CMT1A and ISO CM was observed, indicating no detectable ECM degradation directly at the surface under these conditions. To further refine the ECM mimic, we tested three additional coating strategies: (1) Laminin + DQ collagen type IV, (2) Laminin + DQ collagen type IV with extra DQ collagen type IV added to the medium after 3 hours, and (3) Laminin only, with DQ collagen type IV added later to the medium (***Fig.2A***). Across all three conditions, the coated plates revealed significantly higher fluorescence in CMT1A compared to ISO samples (condition

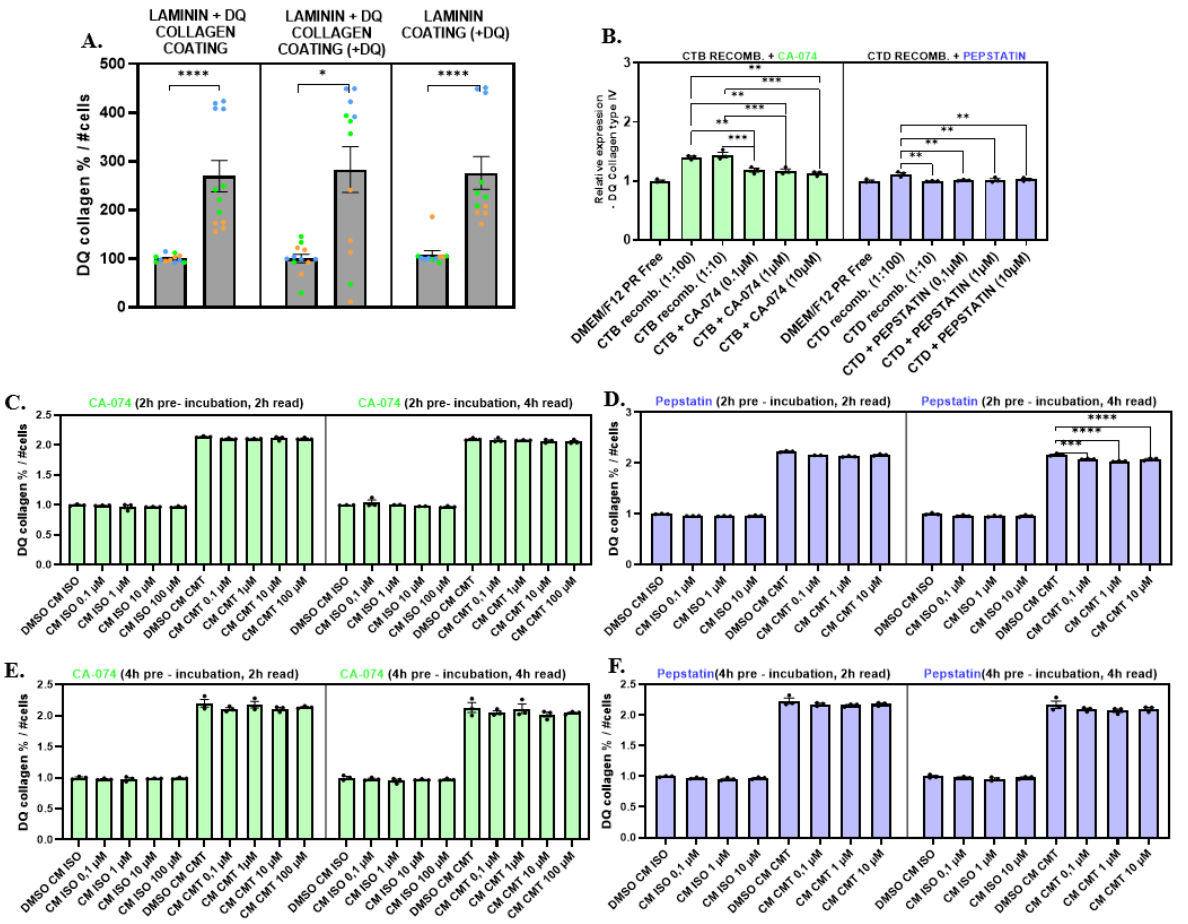

Fig. 2 - DQ-collagen type IV assay reveals enhanced ECM degradation in CMT1A Schwann cells and cathepsin-mediated proteolysis: *(A) Quantification of DQ collagen type IV cleavage under different coating conditions in response to CMT1A versus ISO CM. (B) Recombinant CTB and CTD activity on DQ collagen type IV in the presence or absence of specific inhibitors (CA-074, Pepstatin). (C - F) DQ-collagen type IV degradation measured in ISO and CMT1A CM following pre-incubation with (C, E) CA-074 or (D, F) Pepstatin at various concentrations and time points (two hours vs. four hours). Pepstatin shows partial inhibitory effects. Data are shown as mean ± SEM (n = 3-5). Statistical analysis: One-way ANOVA with Tukey's post hoc or Kruskal-Wallis with Dunn's post hoc. * ($p \leq 0.05$), ** (($p \leq 0.01$), ***($p \leq 0.001$), and ****($p \leq 0.0001$).*

1&3; $p < 0.0001$, condition 2; $p < 0.05$) (***Fig.2A***). Based on these and previously mentioned findings (*Libberecht, K. Unpublished PhD thesis, 2024*), we hypothesized that cathepsins, especially cathepsin B (CTB) and cathepsin D (CTD), might be responsible for this proteolytic activity. A proof-of-concept demonstration of enzymatic function (rather than disease relevance), recombinant CtB and CtD showed robust degradation of DQ-collagen type IV *in vitro*. Incubation with their respective inhibitors confirmed dose-dependent suppression: CA-074 and CA-074Me for CTB, and Pepstatin for CTD. Recombinant CTB showed a highly significant treatment effect ($p < 0.0001$). Statistical analysis confirmed significant inhibition by CA-074 at 0.1 µM ($p = 0.0108$), 1 µM ($p = 0.0180$), and especially 10 µM ($p = 0.0004$), compared to CTB alone. Pepstatin inhibited CTD significantly ($p = 0.0049$), with notable post hoc significance at 0.1–10 µM (p values ranging from 0.0326 to 0.0183) (***Fig. 2B***).

Next, we applied these inhibitors to the CM from ISO and CMT1A iPSC-SCPs. CM was pre-incubated with CA-074 (0.1 - 1 - 10 – 100 µM) or Pepstatin (0.1 – 1 - 10 µM) for two and four hours at 37°C, reflecting the known 5–6h half-life of CTB/CTD. CA-074 treatment resulted in no significant effect on DQ-collagen cleavage in either group ($p > 0.9999$) (***Fig. 2C & 2E***). Pepstatin yielded the only overall statistically significant reduction in CMT1A CM (1 µM; $p < 0.05$, 0.1 µM; $p = 0.0001$; 1 - 10 µM; $p < 0.0001$) after a two hour pre-incubation, but none of the individual comparisons reached significance after multiple testing corrections (***Fig. 2D & 2F***).

Mapping lysosomal and proteolytic mRNA alterations and compensation in C3 nerve tissue - To investigate how lysosomal stress contributes to CMT1A pathology, we analyzed transcriptional changes in sciatic nerves from C3-PMP22 transgenic mice treated with cathepsin inhibitors (CA-074, CA-074Me, and Pepstatin A) or vehicle. Quantitative PCR analysis revealed significant changes in lysosomal and proteolytic genes in the C3 neurodegeneration model. We observed that LAMP-1 expression did not significantly differ between WT and C3 vehicle-treated mice. However, LAMP-1 was significantly reduced following treatment with CA-074 (p = 0.0251 vs. C3), CA-074Me (p = 0.0196), and Pepstatin (p = 0.0222), indicating a suppression of lysosomal membrane components in response to protease inhibition (***Fig 3A***). TFEB, a regulator of lysosomal biogenesis, was significantly upregulated in C3 mice (p = 0.0004) compared to WT. CA-074Me and Pepstatin treatments partially reversed this increase (p = 0.0478 and p = 0.0076 vs. C3, respectively). Interestingly, CA-074 treatment further enhanced TFEB expression (p = 0.0205) (***Fig 3B***). Among the cathepsins, CTB was significantly elevated in C3 mice (p = 0.0022) compared to WT. This elevation was effectively normalized by CA-074 (p = 0.0034), and also significantly reduced by CA-074Me (p = 0.0126) and Pepstatin (p = 0.0335), confirming the inhibitory efficacy on CTB expression (***Fig 3C***). CTD levels were also upregulated in C3 (p = 0.0004) compared to WT, but none of the

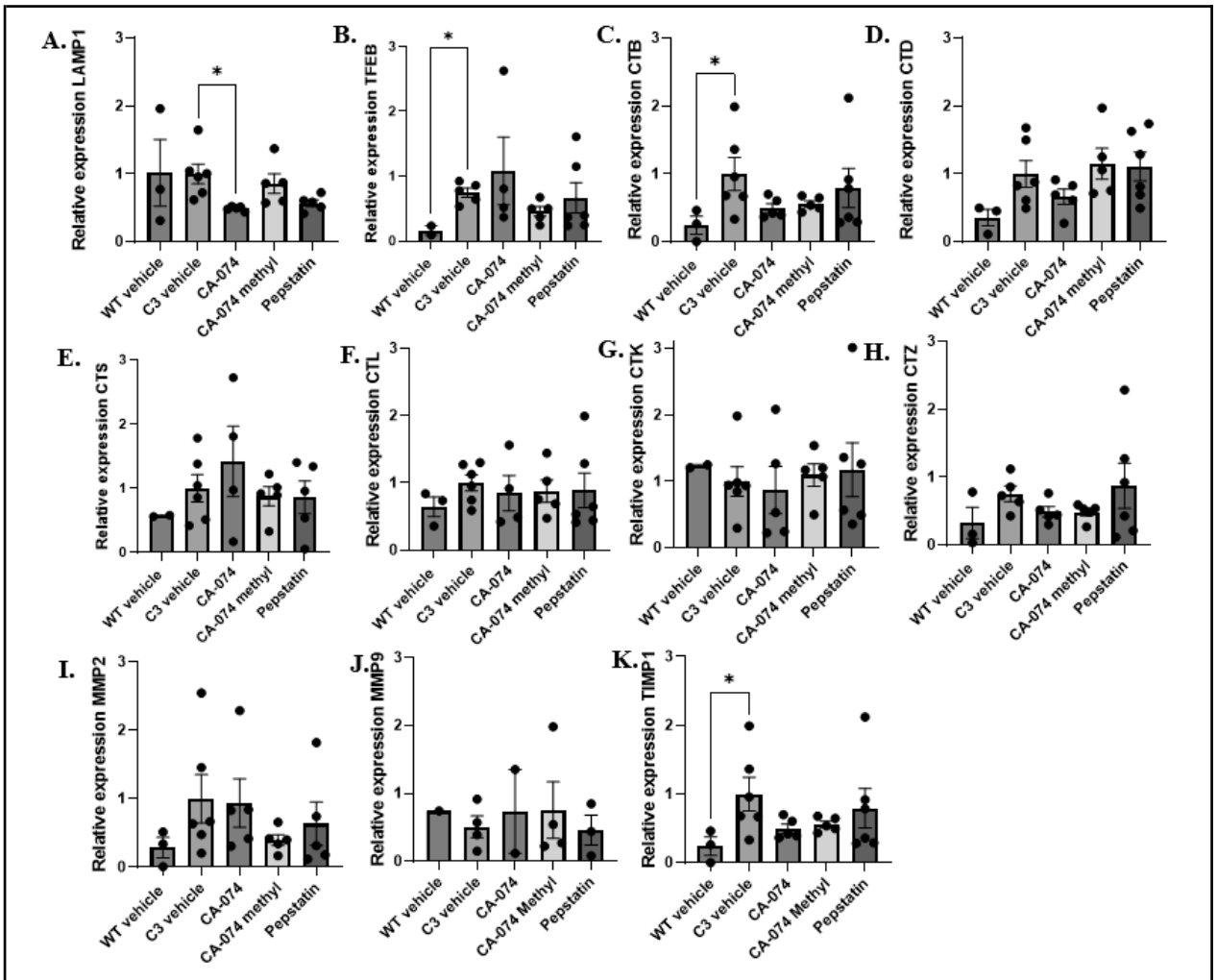

Fig. 3 – Relative mRNA expression levels of lysosomal and proteolytic genes in sciatic nerve tissue after four weeks of treatment: (A - K) *Quantification of gene expression levels for LAMP1, TFEB, CTB, CTD, CTS, CTL, CTK, CTZ, MMP2, MMP9, and TIMP1 across WT, C3 vehicle, and treatment groups (CA-074, CA-0774Me, and Pepstatin). Data are presented as mean ± SEM. Statistical analysis : One-way ANOVA with Tukey's post hoc test. * $p < 0.05$*

treatments significantly altered its expression (***Fig 3D***). CTS expression was increased in C3 mice (p = 0.0026) vs. WT. Treatment with CA-074 paradoxically amplified CTS expression (p = 0.0173 vs. C3), potentially indicating a compensatory proteolytic response. CA-074Me and Pepstatin caused non-significant reductions (***Fig 3E***). In contrast, CTL levels were not significantly changed in C3 compared to WT, but upregulated after CA-074 treatment (p = 0.0138 vs. C3), again supporting a compensatory mechanism. CTL levels after CA-074Me and Pepstatin treatments remained statistically unchanged (***Fig 3F***).
CTK expression remained largely stable across all groups, and no treatment-induced effects were observed (***Fig 3G***). CTZ was upregulated in C3 vs. WT (p = 0.0082), with Pepstatin inducing a further elevation (p = 0.0437 vs. C3), whereas CA-074 and CA-074Me produced non-significant reductions (***Fig 3H***).
Regarding matrix remodeling enzymes, MMP2 was elevated in C3 mice (p = 0.0404) vs. WT, though this elevation was not significantly modulated by CA-074, CA-074Me , or Pepstatin (***Fig 3I***). In contrast, MMP9 was reduced in C3 (p = 0.0144) compared to WT, and this reduction was reversed by CA-074 (p = 0.0067 vs. C3) and CA-074Me (p = 0.0130), but not by Pepstatin (***Fig 3J***). Finally, the MMP inhibitor TIMP1 was significantly upregulated in C3 mice (p = 0.0003) compared to WT. This increase was attenuated by CA-074 (p = 0.0026 vs. C3) and CA-074Me (p = 0.0157), while Pepstatin did not produce a significant change (***Fig 3K***).

Mapping lysosomal and proteolytic protein alterations in C3 nerve tissue – Fluorescence-based protein analysis of sciatic nerves from C3-PMP22 mice treated with cathepsin inhibitors (CA-074, CA-074Me, and Pepstatin A) or vehicle revealed significant changes in lysosomal and ECM markers. Laminin 1+2 showed a significant increase in C3 vehicle-treated mice compared to WT (p = 0.0350), though no statistically significant differences were found between individual treatment groups and the C3 vehicle. Analysis of integrated density further confirmed significant alterations (p = 0.0158), with CA-074-treated animals showing a significant increase compared to C3 vehicle (p = 0.0196) (***Fig 4B***).
Collagen IV staining revealed significant differences in protein levels between groups (p = 0.0022), although statistics did not identify significant differences between the C3 vehicle and any treatment group. Integrated density values were also significantly altered (p = 0.0462), but no post hoc differences reached significance, suggesting a trend toward modulation without clear reversal of C3-associated increases (***Fig 4C***).
LAMP1 expression, assessed by fluorescence, did not differ significantly between groups for either protein level (p = 0.0994) or integrated density (p = 0.1016), consistent with qPCR results showing no major shift in LAMP1 mRNA under baseline or treatment conditions (***Fig 4A***).
CTD fluorescence intensity was significantly increased in C3 mice (p = 0.0004), with strong differences between C3 vehicle and both WT (p < 0.0001) and CA-074-treated animals (p = 0.0076), indicating suppression of CTD at the protein level in response to inhibition (***Fig 2A***). Caspase-3 fluorescence did not significantly differ between groups for protein level (p = 0.5658) and Integrated density (p = 0.2173) (***Fig 4D***). Taken together, the fluorescence analyses indicate subtle and treatment-dependent alterations in lysosomal and proteolytic protein markers in the C3 neurodegeneration model. While statistically significant changes were observed for Laminin 1+2 and CTD following specific inhibitor treatments (notably CA-074 and CA-074Me), other markers such as LAMP1 and Caspase-3 showed no significant differences across groups.

Ultrastructural Changes in Myelination and Axonal Morphology - As part of our *in vivo* study were we evaluated whether cathepsin inhibitors (CA074, CA-074Me, and Pepstatin A) could ameliorate the characteristic hypomyelination and axonal degeneration in sciatic nerves of our treatment groups. While cathepsin inhibition showed modest therapeutic effects, transmission electron microscopy revealed persistent ultrastructural abnormalities across treatment groups.

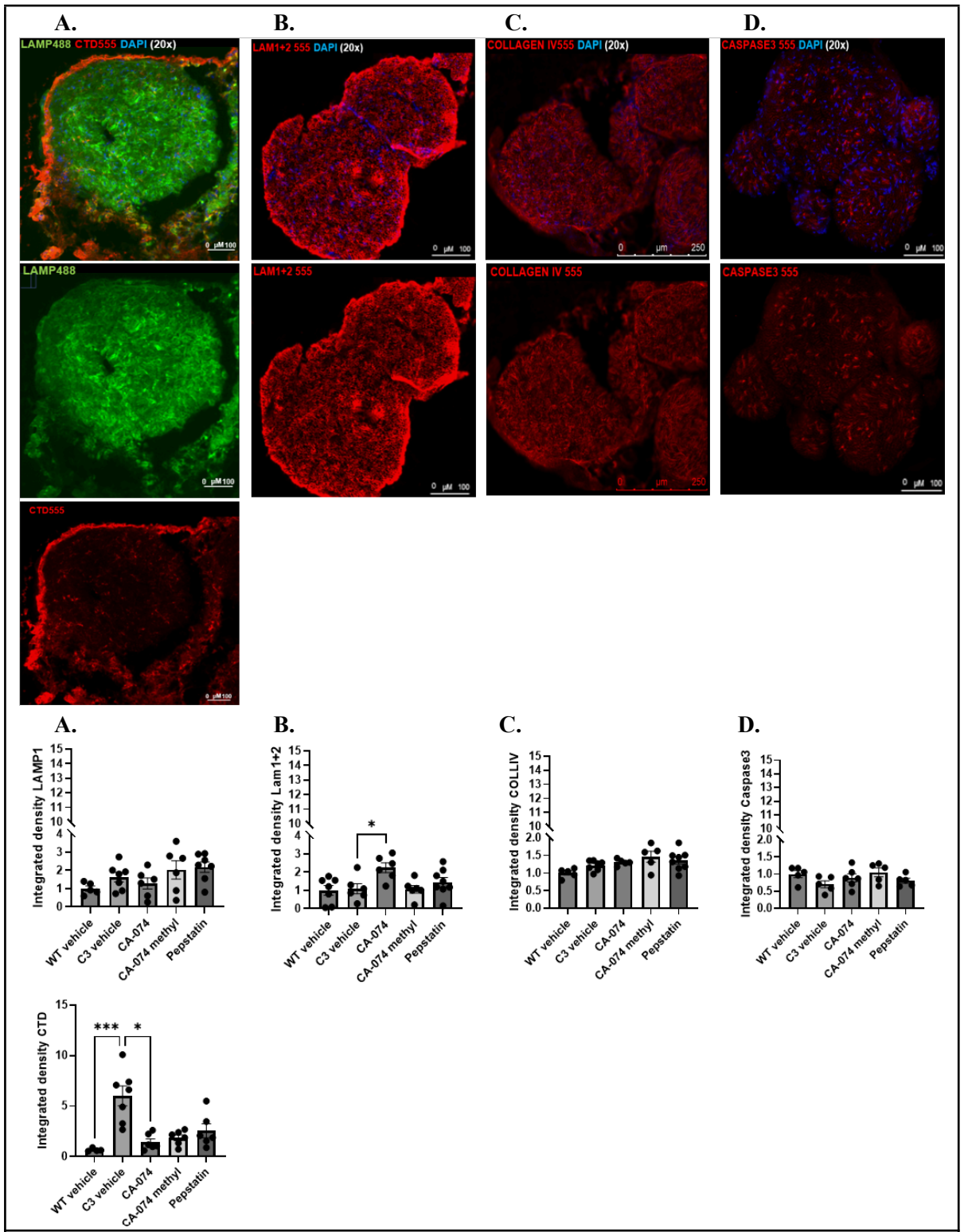

Fig. 4 - Fluorescent-based analysis of lysosomal and proteolytic markers in the C3 neurodegeneration model. *(A) Representative images and quantification of LAMP1 (green) and CTD (red) integrated fluorescence intensity. (B) Laminin 1+2 (red) staining and quantification of integrated density. (C) Collagen IV (red) staining and quantification. (D) Caspase-3 (red) staining and integrated density analysis. Graphs represent mean ± SEM (n = 6-8 per group). Statistical analysis: One-way Anova or Kruskal-Wallis test with Tukey's or Dunn's post hoc correction. * p < 0.05, ***p ≤ 0.001.*

Axon diameter distribution - Axon diameter analysis revealed a unimodal distribution across all groups, with most axons ranging between 2.0 and 5.0 µm and peaking between 3.0–3.5 µm (***Fig 5A***). The overall shape of the distribution was preserved across conditions, suggesting no substantial shifts in axonal size. However, a subset of axons with diameters

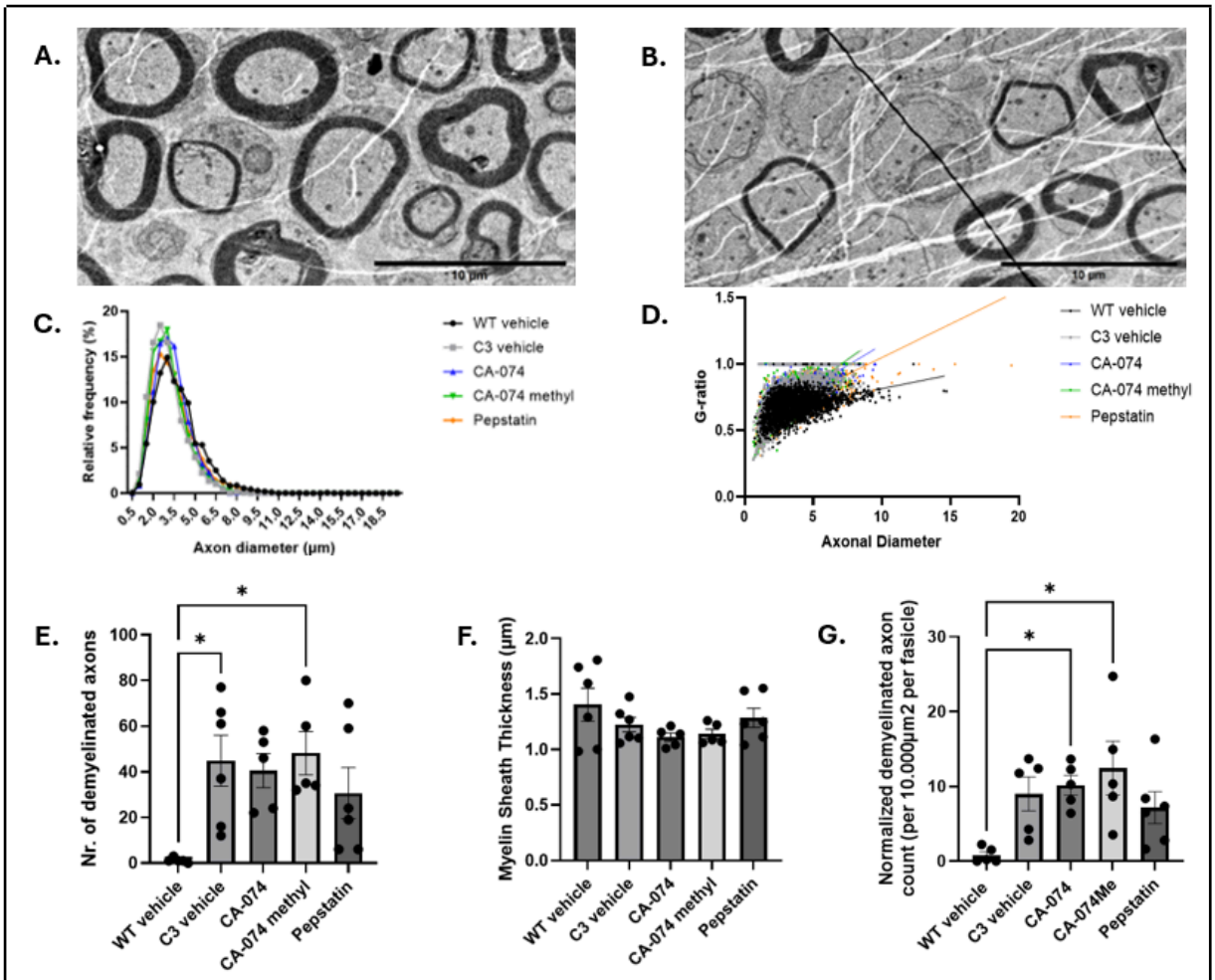

Fig. 5 – Transmission Electron Microscopy Analysis of Sciatic Nerve Demyelination and Axonal Pathology*; (A&B) Representative TEM image of sciatic nerve cross-sections showing demyelinated axons (B) in experimental groups compared to WT groups (A). Scale bar: 10 µm. (C) Axon diameter distribution across experimental groups. (D) G-ratio plots comparing axonal diameter to myelin thickness. (E) Quantification of demyelinated axons. (F) Myelin sheath thickness. (G) Normalized demyelination per 10,000µm². CA-074 (p = 0.0492) and CA-074Me (p = 0.0145) significantly increased demyelination vs. WT. Graphs represent mean ± SEM (n = 5-6 mice per group). Statistical analysis: One-way ANOVA or Kruskal-Wallis test with post hoc Tukey's or Dunn's correction. * p < 0.05.*

<1.0 µm was observed in all groups, potentially indicating axonal atrophy or impaired regeneration. Mean axon diameters were significantly reduced in the C3 vehicle group (3.01 ± 0.02 µm) compared to WT controls (3.75 ± 0.03 µm), reflecting neurodegenerative changes. Treatment with CA-074 (3.36 ± 0.02 µm), CA-074 methyl ester (3.16 ± 0.02 µm), and Pepstatin (3.41 ± 0.03 µm) partially mitigated this reduction but did not fully restore WT levels.

G-ratio analysis - G-ratio (axon diameter / fiber diameter) analysis confirmed the expected inverse relationship between axon diameter and myelin thickness in all groups (***Fig 5B***). Linear regression analysis revealed significantly steeper slopes in C3 vehicle (0.073) and CA-074-treated mice (0.0617) compared to WT (0.0208), suggesting relatively thinner myelin sheaths across a range of axon diameters. R^2 values were also higher in the treated groups (e.g., 0.47 for C3 vehicle) versus WT (0.16), reinforcing the altered myelin dynamics.

Proportion of hypo-myelinated axons - Quantification of axons with G-ratios ≥ 0.8 revealed increased incidence in all experimental groups relative to WT (1.21%). The C3 vehicle group showed a marked elevation (4.70%), with similarly high proportions in CA-074 (4.09%), CA-074Me (4.41%), and Pepstatin (3.62%) groups.These findings suggest treatment-induced or compensatory hypomyelination. Outlier analysis using the ROUT method (Q = 1%) confirmed the biological relevance of these elevated values.

Demyelination (axon counts) - Kruskal-Wallis testing demonstrated significant differences in the number of demyelinated axons across groups (p = 0.0102; ***Fig 5C***). WT vehicle-treated mice displayed minimal demyelination, whereas the C3 vehicle group exhibited significantly higher levels (p = 0.0201 vs. WT). CA-074 methyl ester treatment also showed significant increases relative to WT (p = 0.0163), while CA-074 and Pepstatin groups trended higher but did not reach significance (p = 0.0900 and p = 0.2752, respectively). No significant differences were observed between treatment groups and the C3 vehicle condition.

Myelin Sheath Thickness - Analysis of myelin sheath thickness indicated no significant differences among experimental groups (***Fig 5D***). While thickness measurements showed a tendency toward reduction in C3 vehicle and treatment groups compared to WT controls, these trends did not reach statistical significance. Notably, variance in sheath thickness differed between groups. Pepstatin treatment showed a modest increase in average thickness compared to C3 vehicle controls, though this difference was not significant.

Demyelination normalized by fascicle area - To account for differences in fascicle size, demyelinated axons were normalized per 10,000 µm² (***Fig 5E***). Significant differences were observed between treatment groups (p = 0.0118), with both CA-074 (p = 0.0492) and CA-074Me (p = 0.0145) showing increased demyelination compared to WT controls. While C3 vehicle mice demonstrated elevated demyelination (p = 0.0719 vs WT), the difference did not reach statistical significance. Pepstatin-treated mice showed a non-significant reduction in demyelination compared to C3 vehicle controls (p > 0.9999), potentially indicating mild protective effects.

In vivo* effects of C381 on lysosomal function and Schwann cell integrity in C3-PMP22 mice** - A comprehensive *in vivo* study evaluates the therapeutic potential of C381, a novel lysosomal - modulating compound, in the C3-PMP22 mouse model of CMT1A. Baseline characterization prior to treatment revealed significant differences in both electrophysiological latency and amplitude. Latency measurements differed significantly between groups, as did amplitude values (p < 0.0001) (Fig 6A&B***), indicating group differences prior to intervention. In contrast, baseline body weight did not differ significantly between groups (p = 0.9584) (***Fig 6C***), suggesting a comparable metabolic baseline. Behavioral testing also revealed pre-treatment differences. On the Beam Walk task, significant group differences were present at both bar widths: 12 mm (p < 0.0004) (***Fig 6D***), and 7 mm (p < 0.0001) (***Fig 6E***).
RotaRod performance similarly differed across groups (p < 0.0001), indicating baseline discrepancies in motor coordination (***Fig 6F***). Finally, hanging wire test results showed a significant difference in median coordination (p = 0.0019), suggesting pre-existing variation in grip strength or endurance (***Fig 6G***). This study is conducted over a period of four weeks. Mice will receive intraperitoneal injections of C381 twice weekly. Behavioral assessments will be repeated twice biweekly to monitor treatment-related changes over-time.

DISCUSSION

This study investigates the pathological role of lysosomal stress and cathepsin dysregulation in CMT1A, a demyelinating peripheral neuropathy primarily caused by PMP22 gene duplication. The results underscore a multifaceted interplay between proteostasis collapse, ECM degradation, and Schwann cell dysfunction, offering new insights into potential therapeutic avenues that target lysosomal and cathepsin activity. This study reveals that lysosomal leakage and elevated CtB and CtD levels may contribute to ECM remodeling in CMT1A, though their role appears more complex than initially hypothesized. While recombinant CtB and CtD demonstrated potent ECM-degrading activity in controlled conditions, the partial inhibition observed in CM assays suggests these proteases likely cooperate with other enzymatic systems *in vivo*. Unlike prior studies that focus on general proteostasis collapse, we identify specific lysosomal proteases as extracellular effectors of disease pathology. Furthermore, we provide the comparative *in vitro* and *in vivo* assessment of cathepsin inhibition and introduce C381 as a promising multimodal agent that targets lysosomal integrity and protease activity simultaneously.
One of the central findings is the significant upregulation of lysosomal enzymes -

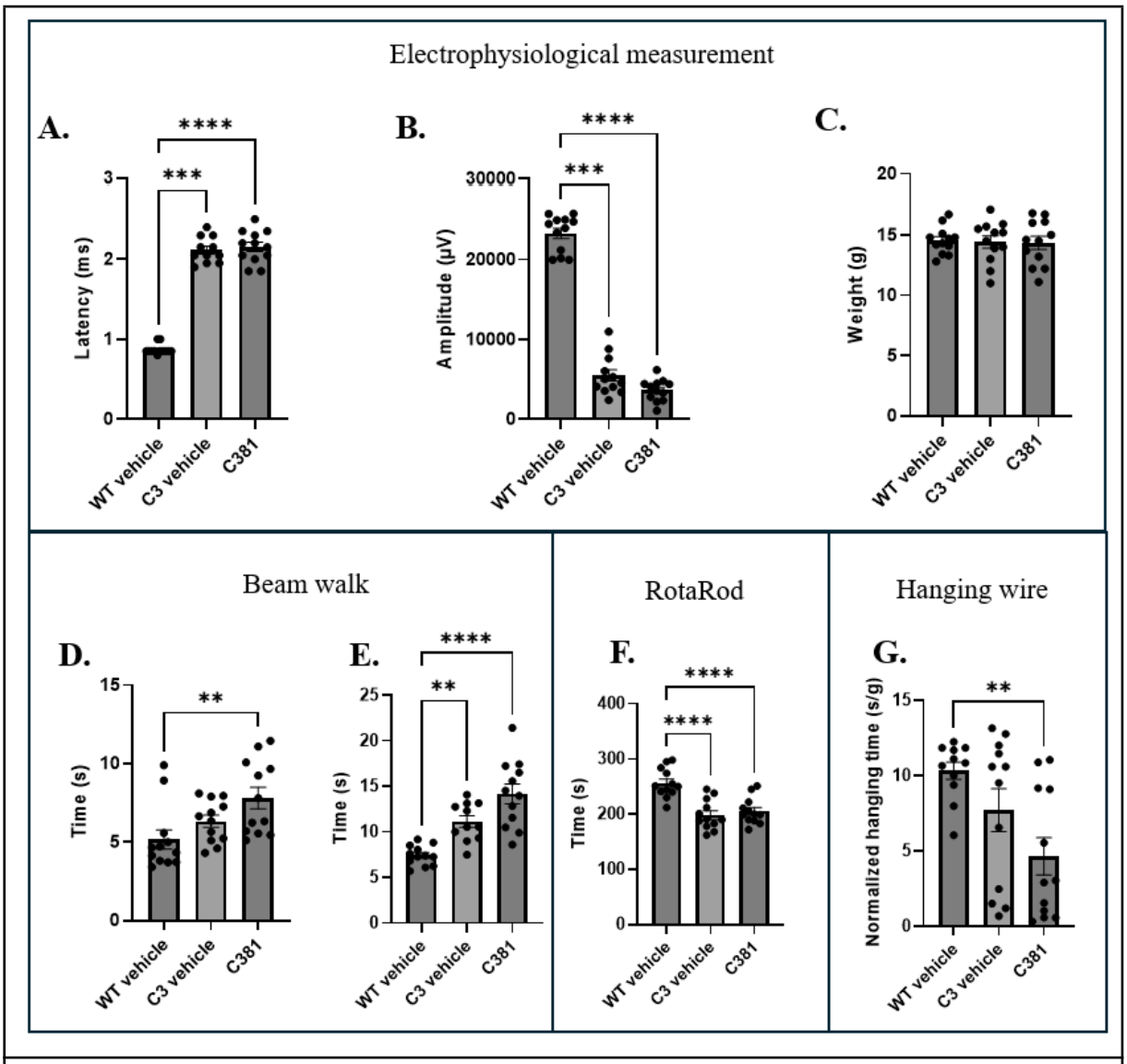

Fig. 6 – Baseline electrophysiological and behavioral measurements in WT and C3 mouse models for the in vivo study with C381; (A-C) *Electrophysiological parameters: (A) Latency, (B) Amplitude, and (C) body weight measured for each treatment group. Significant prolongation of latency and decreased amplitude was measured in C3 mice compared to WT.* ***(D-G)*** *Behavioral tests at baseline: (D) Beam walk (time to cross a 12mm beam), (E) Beam walk (time to cross a 7 mm beam), (F) RotaRod (time in balance and endurance), (G) Hanging wire test (normalised hanging time per gram body weight). C3 mice showed marker motor and coordination deficits relative to WT. Data shown as mean ± SEM (n = 12-13 mice per group). Statistical analysis: One-way ANOVA or Kruskal-Wallis test with post hoc Tukey's or Dunn's correction. ** ($p \leq 0.01$), *** ($p \leq 0.001$), and **** ($p \leq 0.0001$)*

particularly CtB and CtD - in both *in vitro* and *in vivo* CMT1A models. This observation aligns with prior studies suggesting that overexpression of PMP22 leads to protein aggregation, and subsequent activation of compensatory degradation pathways such as the ALP. However, the compensatory capacity of the ALP appears insufficient, as lysosomal stress and membrane permeabilization permit the leakage of active cathepsins into the extracellular space, where they mediate ECM degradation.

These findings are reinforced by a study on CMT2B fibroblasts, where elevated cathepsin activity - especially of CtB, CtD, and CtL - was detected, supporting a broader pattern of lysosomal dysregulation in peripheral neuropathies (46). This cross-validation across CMT subtypes adds robustness to the hypothesis that cathepsin upregulation is a core pathogenic mechanism in CMT1A.

The DQ-collagen degradation assays robustly demonstrated that conditioned medium (CM) from CMT1A Schwann cell precursors (iPSC-SCPs) possess enhanced proteolytic activity compared to isogenic controls. The significant difference in fluorescence intensity following incubation with DQ-collagen

strongly implicates secreted proteases - most likely cathepsins - in ECM remodeling. This extracellular activity is pathological, as it disrupts axo-glial junction and destabilizes the myelination-axon complex, both of which are critical for peripheral nerve function. Supporting this, studies show that CtB and CtD are capable of degrading key ECM components such as Collagen IV, fibronectin, and laminin - proteins that are essential to maintaining nerve structure and Schwann cell interactions (47). This highlights a plausible mechanistic link between lysosomal dysfunction and ECM disruption in CMT1A.

Interestingly, while recombinant cathepsin inhibition (using CA-074, CA-074Me, and Pepstatin) showed clear suppression of collagen degradation in controlled assays, this inhibitory effect was less pronounced in conditioned medium from CMT1A cells. This discrepancy may reflect differences in enzyme accessibility, enzyme stability, or additional unidentified proteases contributing to ECM remodeling. Furthermore, while cathepsin inhibitors significantly altered expression levels of key lysosomal markers *in vivo* - such as LAMP1 and TFEB - the partial normalization of gene expression did not fully reverse structural of functional neuropathology, suggesting that inhibition of individual enzymes may be insufficient to arrest disease progression.

The *in vivo* component of the study using the C3-PMP22 mouse model provided compelling evidence for cathepsin-mediated nerve degeneration. Transmission electron microscopy revealed reduced axon diameters, increased G-ratios (indicative of thinner myelin sheaths), and higher counts of demyelinated axons in C3 mice compared to wild-type controls. Treatment with cathepsin inhibitors led to only partial improvements in these metrics, with some measures, such as hypomyelination, persisting despite pharmacological intervention. These findings align with broader literature where cathepsin inhibition, although beneficial in reducing tissue degeneration, often does not reverse existing structural damage, as observed in neurodegenerative and cancer models (47). This suggests the importance of early intervention and potentially combinatorial approaches.

The small molecule C381 offers a broader therapeutic benefit by restoring lysosomal acidification and reducing ER stress. Although not fully tested in this study, its previously reported effects - activation of TGF-β signaling, enhancement of lysosomal acidification, and attenuation of ER stress - target multiple intersecting pathways relevant to CMT1A pathology. The potential of C381 to alleviate the PERK-mediated stress response and promote Schwann cell survival represents an encouraging direction for future preclinical trials. Notably, compounds like C381 that modulate upstream regulatory mechanisms may yield broader efficacy than cathepsin inhibitors that act downstream in the pathological cascade.

Beyond small molecules, recent advances in gene silencing approaches targeting PMP22 via siRNA have shown substantial success in reducing PMP22 expression and restoring myelination in mouse models of CMT1A (48). These approaches may complement C381's lysosomal benefits by targeting upstream protein accumulation directly.

Moreover, This study demonstrates the value of combining iPSC-derived Schwann cell precursors with murine models. While rodent models alone have struggled to replicate the full spectrum of human CMT1A pathology and treatment responses, human iPSC-SCPs enable disease modeling in a patient-specific, genetically accurate context. This approach provides a powerful platform for dissecting molecular mechanisms and screening candidate therapeutics before moving to *in vivo* validation.

Nonetheless, some limitations merit consideration. The partial rescue of pathological markers upon cathepsin inhibition suggests potential redundancy among proteases or compensatory activation of parallel degradative pathways. Additionally, the effects of long-term inhibition of lysosomal enzymes remain unclear. Given their central role in intracellular degradation and immune regulation, chronic inhibition could introduce unforeseen adverse effects. Therefore, future studies should assess systemic toxicity, immune responses, and the pharmacokinetic profiles of inhibitors in preclinical models.

In summary, this study reveals a pivotal role for lysosomal dysfunction and cathepsin-mediated ECM remodeling in the progression of CMT1A. These findings are corroborated by literature across multiple disease models, confirming that cathepsins are

key players in ECM breakdown and neural degeneration. While targeting CtB and CtD demonstrates potential, especially in ameliorating proteolytic stress, a broader therapeutic strategy - possibly involving agents like C381 or PMP22-silencing RNAi - may be required to halt or reverse nerve degeneration. These findings enrich our understanding of the complex molecular underpinnings of CMT1A and lay the groundwork for the development of multifaceted, mechanism-based therapies.

CONCLUSION

This study demonstrates that lysosomal dysfunction and cathepsin upregulation - particularly of CtB and CtD - drive ECM degradation and Schwann cell pathology in CMT1A. These findings reveal that overexpression of PMP22 disrupts proteostasis and lysosomal integrity, triggering the release of active proteases into the extracellular environment, where they contribute to ECM remodeling and axo-glial destabilization. Although pharmacological inhibition of cathepsins reduced proteolytic activity and partially improved molecular and structural markers, it did not reverse myelin damage or restore nerve function, underscoring the complexity of CMTA pathogenesis. These results suggest that targeting cathepsins alone is insufficient to halt disease progression. Future research should focus on combinatorial strategies that address both upstream drivers, such as ER stress, and downstream effectors like lysosomal leakage and protease activation. Small molecules like C381, which enhance lysosomal homeostasis, represent promising candidates for broader therapeutic intervention. Combining human iPSC-derived Schwann cell models with *in vivo* validation will be essential to advancing these findings toward clinical application.

REFERENCES

1. Harel T, Lupski J. Charcot–Marie–Tooth disease and pathways to molecular based therapies. Clinical genetics. 2014;86(5):422-31.
2. Pisciotta C, Shy ME. Hereditary neuropathy. Handb Clin Neurol. 2023;195:609-17.
3. El-Abassi R, England JD, Carter GT. Charcot-Marie-Tooth disease: an overview of genotypes, phenotypes, and clinical management strategies. PM&R. 2014;6(4):342-55.
4. Casasnovas C, Cano LM, Albertí A, Céspedes M, Rigo G. Charcot-Marie-tooth disease. Foot & Ankle Specialist. 2008;1(6):350-4.
5. Krajewski KM, Lewis RA, Fuerst DR, Turansky C, Hinderer SR, Garbern J, et al. Neurological dysfunction and axonal degeneration in Charcot–Marie–Tooth disease type 1A. Brain. 2000;123(7):1516-27.
6. Li J, Parker B, Martyn C, Natarajan C, Guo J. The PMP22 gene and its related diseases. Molecular neurobiology. 2013;47:673-98.
7. Uchoa Cavalcanti EB, Santos SCdL, Martins CES, de Carvalho DR, Rizzo IMPdO, Freitas MCDNB, et al. Charcot‐Marie‐Tooth disease: Genetic profile of patients from a large Brazilian neuromuscular reference center. Journal of the Peripheral Nervous System. 2021;26(3):290-7.
8. Prior R, Silva A, Vangansewinkel T, Idkowiak J, Tharkeshwar AK, Hellings TP, et al. PMP22 duplication dysregulates lipid homeostasis and plasma membrane organization in developing human Schwann cells. Brain. 2024;147(9):3113-30.
9. Marinko JT, Carter BD, Sanders CR. Direct relationship between increased expression and mistrafficking of the Charcot–Marie–Tooth–associated protein PMP22. Journal of Biological Chemistry. 2020;295(34):11963-70.
10. Notterpek L, Ryan MC, Tobler AR, Shooter EM. PMP22 accumulation in aggresomes: implications for CMT1A pathology. Neurobiology of disease. 1999;6(5):450-60.
11. Chittoor VG, Sooyeon L, Rangaraju S, Nicks JR, Schmidt JT, Madorsky I, et al. Biochemical characterization of protein quality control mechanisms during disease progression in the C22 mouse model of CMT1A. ASN neuro. 2013;5(5):AN20130024.
12. Fortun J, Go JC, Li J, Amici SA, Dunn Jr WA, Notterpek L. Alterations in degradative pathways and protein aggregation in a neuropathy model based on PMP22 overexpression. Neurobiology of disease. 2006;22(1):153-64.
13. Zhang Z, Yue P, Lu T, Wang Y, Wei Y, Wei X. Role of lysosomes in physiological activities, diseases, and therapy. Journal of hematology & oncology. 2021;14(1):79.
14. Ferrari V, Tedesco B, Cozzi M, Chierichetti M, Casarotto E, Pramaggiore P, et al. Lysosome quality control in health and neurodegenerative diseases. Cellular & Molecular Biology Letters. 2024;29(1):116.
15. Machado E, White-Gilbertson S, van de Vlekkert D, Janke L, Moshiach S, Campos Y, et al. Regulated lysosomal exocytosis mediates cancer progression. Science advances. 2015;1(11):e1500603.
16. Niemann A, Berger P, Suter U. Pathomechanisms of mutant proteins in Charcot-Marie-Tooth disease. Neuromolecular medicine. 2006;8:217-41.
17. Schlebach JP, Narayan M, Alford C, Mittendorf KF, Carter BD, Li J, et al. Conformational stability and pathogenic misfolding of the integral membrane protein PMP22. Journal of the American Chemical Society. 2015;137(27):8758-68.
18. Almanza A, Carlesso A, Chintha C, Creedican S, Doultsinos D, Leuzzi B, et al. Endoplasmic reticulum stress signalling–from basic mechanisms to clinical applications. The FEBS journal. 2019;286(2):241-78.
19. Corazzari M, Gagliardi M, Fimia GM, Piacentini M. Endoplasmic reticulum stress, unfolded protein response, and cancer cell fate. Frontiers in oncology. 2017;7:78.
20. Adams CJ, Kopp MC, Larburu N, Nowak PR, Ali MM. Structure and molecular mechanism of ER stress signaling by the unfolded protein response signal activator IRE1. Frontiers in molecular biosciences. 2019;6:11.
21. Wu X, Rapoport TA. Mechanistic insights into ER-associated protein degradation. Current opinion in cell biology. 2018;53:22-8.

22. Krshnan L, van de Weijer ML, Carvalho P. Endoplasmic reticulum–associated protein degradation. Cold Spring Harbor Perspectives in Biology. 2022;14(12):a041247.
23. Hwang J, Qi L. Quality control in the endoplasmic reticulum: crosstalk between ERAD and UPR pathways. Trends in biochemical sciences. 2018;43(8):593-605.
24. Senft D, Ze'ev AR. UPR, autophagy, and mitochondria crosstalk underlies the ER stress response. Trends in biochemical sciences. 2015;40(3):141-8.
25. Ma Y, Hendershot LM. The unfolding tale of the unfolded protein response. Cell. 2001;107(7):827-30.
26. Lee S, Bazick H, Chittoor-Vinod V, Al Salihi MO, Xia G, Notterpek L. Elevated peripheral myelin protein 22, reduced mitotic potential, and proteasome impairment in dermal fibroblasts from Charcot-Marie-Tooth disease type 1A patients. The American journal of pathology. 2018;188(3):728-38.
27. Fortun J, Dunn WA, Joy S, Li J, Notterpek L. Emerging role for autophagy in the removal of aggresomes in Schwann cells. Journal of Neuroscience. 2003;23(33):10672-80.
28. Fortun J, Verrier JD, Go JC, Madorsky I, Dunn WA, Notterpek L. The formation of peripheral myelin protein 22 aggregates is hindered by the enhancement of autophagy and expression of cytoplasmic chaperones. Neurobiology of disease. 2007;25(2):252-65.
29. Trivedi PC, Bartlett JJ, Pulinilkunnil T. Lysosomal biology and function: modern view of cellular debris bin. Cells. 2020;9(5):1131.
30. Vizovišek M, Fonović M, Turk B. Cysteine cathepsins in extracellular matrix remodeling: Extracellular matrix degradation and beyond. Matrix Biology. 2019;75:141-59.
31. Wang F, Gómez‐Sintes R, Boya P. Lysosomal membrane permeabilization and cell death. Traffic. 2018;19(12):918-31.
32. Turk V, Stoka V, Vasiljeva O, Renko M, Sun T, Turk B, et al. Cysteine cathepsins: from structure, function and regulation to new frontiers. Biochimica et Biophysica Acta (BBA)-Proteins and Proteomics. 2012;1824(1):68-88.
33. Yadati T, Houben T, Bitorina A, Shiri-Sverdlov R. The ins and outs of cathepsins: physiological function and role in disease management. Cells. 2020;9(7):1679.
34. Lu P, Takai K, Weaver VM, Werb Z. Extracellular matrix degradation and remodeling in development and disease. Cold Spring Harbor perspectives in biology. 2011;3(12):a005058.
35. Stotz S, Bleher D, Kalbacher H, Maurer A. Grassystatin-derived peptides selectively inhibit cathepsin e and have low affinity to cathepsin d. Biochemical and Biophysical Research Communications. 2020;527(1):238-41.
36. Liaudet-Coopman E, Beaujouin M, Derocq D, Garcia M, Glondu-Lassis M, Laurent-Matha V, et al. Cathepsin D: newly discovered functions of a long-standing aspartic protease in cancer and apoptosis. Cancer letters. 2006;237(2):167-79.
37. Hossain MI, Marcus JM, Lee JH, Garcia PL, Singh V, Shacka JJ, et al. Restoration of CTSD (cathepsin D) and lysosomal function in stroke is neuroprotective. Autophagy. 2021;17(6):1330-48.
38. Yoon MC, Solania A, Jiang Z, Christy MP, Podvin S, Mosier C, et al. Selective neutral pH inhibitor of cathepsin B designed based on cleavage preferences at cytosolic and lysosomal pH conditions. ACS chemical biology. 2021;16(9):1628-43.
39. Li L, Nguyen A, Zhao B, Vest R, Yerra L, Sun B, et al. Small Molecule Drug C381 Attenuates Brain Vascular Damage Following Repetitive Mild Traumatic Injury. Neurotrauma Reports. 2024;5(1):1016-26.
40. Vest RT, Chou C-C, Zhang H, Haney MS, Li L, Laqtom NN, et al. Small molecule C381 targets the lysosome to reduce inflammation and ameliorate disease in models of neurodegeneration. Proceedings of the National Academy of Sciences. 2022;119(11):e2121609119.
41. Jerath NU, Shy ME. Hereditary motor and sensory neuropathies: Understanding molecular pathogenesis could lead to future treatment strategies. Biochimica et Biophysica Acta (BBA)-Molecular Basis of Disease. 2015;1852(4):667-78.
42. Juneja M, Burns J, Saporta MA, Timmerman V. Challenges in modelling the Charcot-Marie-Tooth neuropathies for therapy development. Journal of Neurology, Neurosurgery & Psychiatry. 2019;90(1):58-67.

43. Huxley C, Passage E, Manson A, Putzu G, Figarella-Branger D, Pellissier J, et al. Construction of a mouse model of Charcot-Marie-Tooth disease type 1A by pronuclear injection of human YAC DNA. Human molecular genetics. 1996;5(5):563-9.
44. Fledrich R, Stassart RM, Sereda MW. Murine therapeutic models for Charcot-Marie-Tooth (CMT) disease. British medical bulletin. 2012;102(1):89-113.
45. Shi L, Huang L, He R, Huang W, Wang H, Lai X, et al. Modeling the pathogenesis of Charcot-Marie-Tooth disease type 1A using patient-specific iPSCs. Stem Cell Reports. 2018;10(1):120-33.
46. Romano R, Rivellini C, De Luca M, Tonlorenzi R, Beli R, Manganelli F, et al. Alteration of the late endocytic pathway in Charcot–Marie–Tooth type 2B disease. Cellular and Molecular Life Sciences. 2021;78:351-72.
47. Victor BC, Anbalagan A, Mohamed MM, Sloane BF, Cavallo-Medved D. Inhibition of cathepsin B activity attenuates extracellular matrix degradation and inflammatory breast cancer invasion. Breast Cancer Research. 2011;13:1-14.
48. Boutary S, Caillaud M, El Madani M, Vallat J-M, Loisel-Duwattez J, Rouyer A, et al. Squalenoyl siRNA PMP22 nanoparticles are effective in treating mouse models of Charcot-Marie-Tooth disease type 1 A. Communications Biology. 2021;4(1):317.

Acknowledgements – The author gratefully acknowledges the support of the Research Foundation Flanders (FWO Vlaanderen) for funding this research project. JM would like to especially thank HJ for het guidance, feedback, and encouragement throughout the entire internship and this thesis process. JM would also like to thank KL and HJ for their scientific input, technical support, and valuable discussions. The author is further grateful to the entire FIERCE lab at UHasselt for creating a collaborative and motivating research environment.

Author contributions – EW and HJ designed the research and supervised the project. JM carried out all *in vitro* and *in vivo* experiments under supervision of HJ, and performed data collection and analysis under the supervision of KL and HJ. The patient-derived iPSC-SCP lines and isogenic controls were kindly provided by LVDB. JM prepared the figures and wrote the thesis manuscript, with critical revisions and editing provided by HJ. All authors reviewed and approved the final version of the work. AI was used for language refinement during manuscript preparation.

Supplementary information

Supplementary Table 1 - qPCR primer sequences.

Gene	Species	Primer pair sequence	
		Forward sequence (5'-3')	**Reverse Sequence (5'-3')**
LAMP1	Mouse	GGT AAC AAC GGA ACC TGCT	TCT GGT CAC CGT CTT GTT GT
CTB	Mouse	CGG CTC TTG TTG GGC ATT TG	GAC TCG GCC ATT GGT GTG AA
CTD	Mouse	TAC ACG CTC AAG GTG TCG C	GTG TAG TAG CGG CCG ATG AA
CTZ	Mouse	GGC CAG ACT TGC TAC CAT CC	ACA CCG TTC ACA TTT CTC CAG
CTL	Mouse	ATC AAA CCT TTA GTG CAG AGT GG	CTG TAT TCC CCG TTG TGT AGC
CTS	Mouse	CCA TTG GGA TCT CTG GAA GAA AA	TCA TGC CCA CTT GGT AGG TAT
CTK	Mouse	GGG CCA GGA TGA AAG TTG TA	CAC TGC TCT CTT CAG GGC TT
TFEB	Mouse	GAC TCA GAA GCG AGA GCT AAC A	CCT GCG TCT TCT CTC AAT TAG GT
MMP2	Mouse	GAT GCT TTT GCT CGG GCC TT	GTA TCC ATC TCC ATG CTC CCA
MMP9	Mouse	GGG CTT AGA TCA TTC GAG CGT	CGT TAG AGC CAC GAC CAT ACA
TIMP1	Mouse	GGACC TGGT CATAAG CTA	TAC CGG ATA TCT GCG GCA TT

Supplementary Table 2 - Primary antibodies for IHC.

Target	Species	Dilution	Reference
LAMP-1	Rat	1:200	Sc-19992
CTB	Rabbit	1:200	Ab125067
CTD	Rabbit	1:300	Ab75852
Cleaved Caspase3	Rabbit	1:400	(D175)(5A1E)
Laminin 1+2	Rabbit	1:250	Ab7463
Collagen IV	Rabbit	1:450	Ab6586

List of abbreviations

Abbreviation	Full Term
CMT	Charcot-Marie-Tooth disease
CMT1A	Charcot-Marie-Tooth disease type 1A
PMP22	Peripheral Myelin Protein 22
ECM	Extracellular Matrix
CtB	Cathepsin B
CtD	Cathepsin D
CtL	Cathepsin L
CtK	Cathepsin K
CtS	Cathepsin S
CtZ	Cathepsin Z
MMP2	Matrix Metalloproteinase 2
MMP9	Matrix Metalloproteinase 9
TIMP1	Tissue Inhibitor of Metalloproteinase 1
ALP	Autophagy-Lysosomal Pathway
iPSC	Induced Pluripotent Stem Cell
SCP	Schwann Cell Precursor
qPCR	Quantitative Polymerase Chain Reaction
DQ	Dye-Quenched
CM	Conditioned Medium
ISO	Isogenic Control
CA-074	Cathepsin B inhibitor (Extracellular)
CA-074Me	Cathepsin B inhibitor (Intracellular)
DMSO	Dimethyl Sulfoxide
PEG300	Polyethylene Glycol 300
TEM	Transmission Electron Microscopy
SEM	Standard error of the mean